# Photocatalytic Patterning and Modification of Graphene

Liming Zhang,[†] Shuo Diao,[†] Yufeng Nie,[†] Kai Yan,[†] Nan Liu,[†] Boya Dai,[†] Qin Xie,[†] Alfonso Reina,[‡,§] Jing Kong,[‡] and Zhongfan Liu*,[†]

[†]Centre for Nanochemistry, Beijing National Laboratory for Molecular Sciences, State Key Laboratory for Structural Chemistry of Unstable and Stable Species, College of Chemistry & Molecular Engineering, Peking University, Beijing 100871, People's Republic of China

[‡]Department of Materials Science &Engineering, and Electrical Engineering & Computer Sciences, Massachusetts Institute of Technology, Cambridge, Massachusetts 02139, United States

S *Supporting Information*

ABSTRACT: TiO_2-based photocatalysis has been widely used to decompose various organic pollutants for the purpose of environmental protection. Such a "green" photochemical process can ultimately degrade organic compounds into CO_2 and H_2O under ambient conditions. We demonstrate here its extended application on the engineering of single- or few-layer graphene. Using a patterned TiO_2 photomask, we have achieved various photochemical tailorings of graphene, including ribbon cutting, arbitrary patterning on any substrate, layer-by-layer thinning, and localized graphene to graphene oxide conversion.

UV−visible spectroscopic studies indicate that the photogenerated, highly reactive ·OH radicals work as sharp chemical scissors. Being a solution-free, cost-effective, scalable, and easy handling technique, the presented photocatalytic patterning and modification approach allows for the versatile design and fabrication of graphene-based devices and circuits, compatible with current microelectronic technology, as demonstrated by this fabricated all-carbon field effect transistor (FET) array.
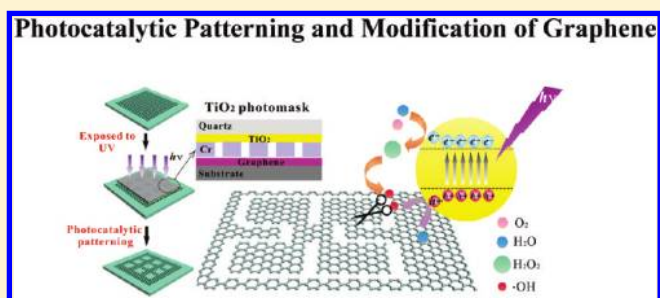
■ INTRODUCTION

Graphene, a two-dimensional (2D) sp^2 carbon network, has attracted a wide range of interests due to its fascinating electronic, mechanical, and thermal properties since 2004.[1,2] The extremely high carrier mobility, mechanical flexibility, optical transparency, and chemical stability of graphene provide a great opportunity for the development of high-performance electronic devices.[3,4] The challenge of graphene electronics arises from its zero bandgap nature as a semimetallic Dirac material.[5] An effective way to open the bandgap in a well-controlled manner and to tailor the 2D graphene sheet into device/circuit architectures is needed.[6] Formation of nanoribbons[5,7,8] and nanomeshes[9−11] has been proven to generate bandgaps in the electronic structure of graphene, with the gap size being dependent on the ribbon width and on the mesh density, respectively. Up to now, in addition to the conventional electron beam lithography,[5] a number of nontraditional techniques have been developed for engineering the graphene sheet, including STM/AFM nanolithography,[12,13] metal nanoparticle-guided directional hydrogenation[14−16] or oxidation,[17] and nanosphere[18]/block copolymer[10,11]/nanowire[19]-masked plasma etching. The limited controllability and/or lack of scalability as well as the complicated and time-consuming procedures of these approaches call for more effort and breakthrough on graphene engineering for graphene electronics.

The TiO_2-based photocatalytic reaction has been widely applied for materials used in daily life for environmental protection, namely TiO_2-coated smart glass, tile, and paint having self-cleaning, antifogging, self-sterilizing, deodorizing, and air-cleaning functions.[20−22] The excellent performance of TiO_2 originates from its strong reactivity under light illumination; many organic pollutants and bacteria can be decomposed to CO_2 and H_2O under ambient conditions.[23,24] The photostability, chemically and biologically inert nature, low cost, and nontoxicity give TiO_2 a great advantage over other photocatalysts.[25] Generally, the photocatalytic reaction starts from the generation of electrons and holes under irradiation of light matched with the bandgap energy of TiO_2 photocatalyst. The photoexcited high energy electrons and holes further react with the surrounding water moisture and oxygen molecules, creating reactive intermediate species, e.g., $\cdot OH$, $O_2^{\bullet -}$, and H_2O_2.[26] The organics in the close vicinity are finally degraded by these reactive intermediates.[21,23,24] Now the question is whether such chemical scissors can be employed to cut the stable sp^2 carbon network of graphene? The present work has given a clear, positive answer. Figure 1a shows the schematic illustration of TiO_2-based photocatalytic technique for engineering single- or few-layer graphene. By simply using a patterned TiO_2 photomask, we can tailor the graphene sheet into any shape on arbitrary substrates with the feature size being determined by the photomask. More importantly, both physical and chemical tailoring can be performed,
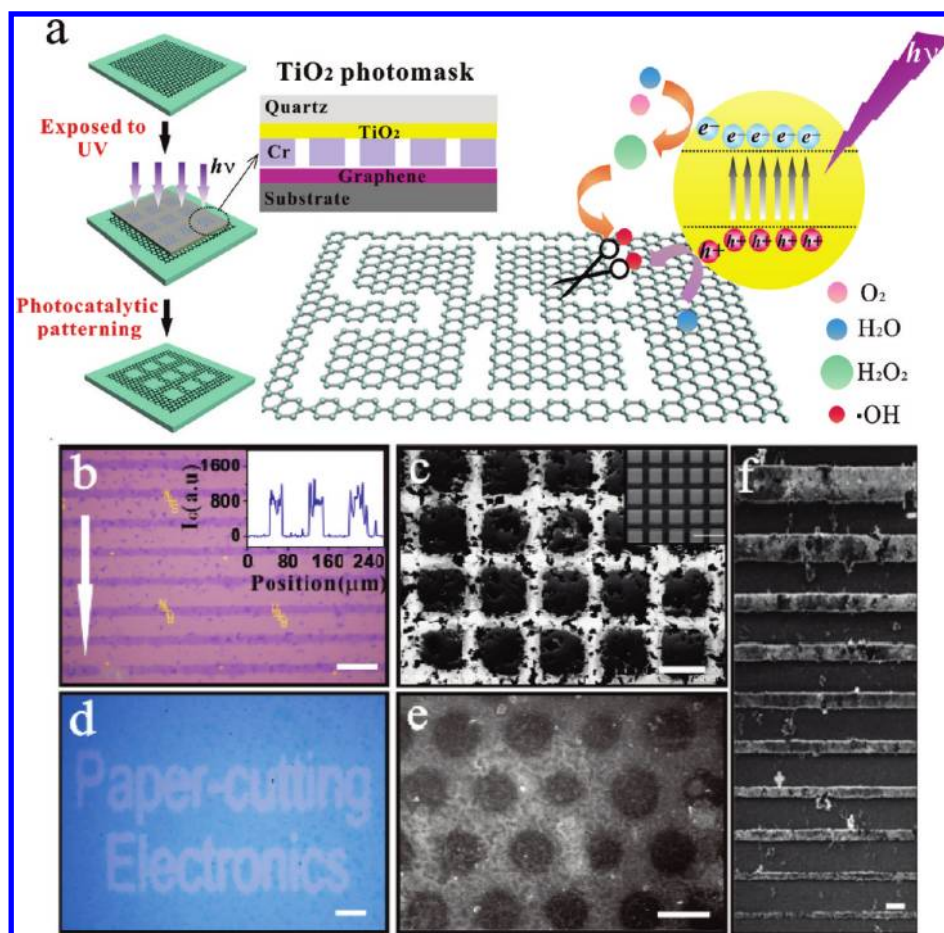
Figure 1. Photocatalytic patterning of graphene. (a) Schematic illustration of the photocatalytic approach to engineering single- or few-layer graphene, in which the quartz plate/TiO_2 thin film/patterned Cr photomask is put into contact with graphene. Under UV illumination, e^- and h^+ are generated on the TiO_2 photomask that further react with the surrounding H_2O and O_2 molecules, producing highly reactive $\cdot$OH radicals, which function as chemical scissors to tailor the graphene sheet in a well-controlled manner. (b) Optical microscope image of graphene ribbons obtained with a line-shape TiO_2 photomask. The inset shows the peak intensity change of the Raman G band of a segregated graphene along the arrow direction. (c) SEM image of a photocatalytically patterned CVD-graphene, in which the inset shows the photomask structure. (d) Optical microscope image of a patterned reduced graphene oxide (RGO) film, illustrating the feasibility of complex structural design. (e) SEM image of a periodically patterned RGO film. (f) SEM image of a series of CVD-graphene ribbons having different widths. The photocatalytic patterning was carried out on SiO_2/Si substrate in b–d, f and on poly(ethylene terephthalate) (PET) in e. Scale bars: 50 μm (b–e), 100 μm (inset of c), 10 μm (f).

controlled by the extent of photocatalytic reaction. The former denotes the actual cutting of the graphene sheet into pieces while the latter is a chemical patterning with the photoexposed area being converted to insulating graphene oxide (GO). The out-of-plane photocatalytic reaction rate on thick graphite is remarkably slower than the in-plane reaction rate, which enables the layer-by-layer thinning of few-layer graphene. Such kinds of versatile photochemical tailoring would offer a fascinating tool for graphene electronics.

■ EXPERIMENTAL SECTION

Fabrication of the TiO_2 Photomask. A Ti (99.999%) layer of 5–15 nm was evaporated onto a quartz plate using a thermal evaporation system (UNIVEX-300, Oerlikon Leybold) with a deposition rate of 0.1–0.3 Å/s, which was followed by calcination in air at 600 °C for 1 h to obtain the TiO_2 film. The quartz plates were precleaned with acetone and water, followed by UV illumination for 10 min to remove organic contaminants. A designed Cr pattern having a typical thickness of 75–90 nm was fabricated on a TiO_2/quartz plate via conventional photolithography and thermal evaporation. The typical photomask used

for cutting and patterning of graphene in this work has a sandwiched structure, including patterned Cr/TiO_2 film/quartz plate. For comparison, we also fabricated a patterned TiO_2 film/quartz plate photomask using the same photolithography procedure.

Sample Preparation. Three types of graphene samples were employed in this work, CVD-graphene, segregated graphene, and reduced graphene oxide (RGO). CVD-graphene was grown on Ni film/SiO_2/Si wafer or Cu foil by chemical vapor deposition (CVD) following the previously reported method.[27,28] The growth on Ni was performed in an ambient pressure CVD system at 900 or 1000 °C with a 5–25 and 1500 sccm flow of CH_4 and H_2, respectively, for 5–10 min. The growth on Cu was carried out at temperatures up to 1000 °C by CVD using a mixture of 35 sccm CH_4 and 2 sccm H_2 at a total pressure of 500 mTorr. Segregated graphene was obtained by vacuum-annealing Ni film using the segregation technique we developed recently.[29] Typically, a Ni film of 150–300 nm containing a trace amount of carbon impurity was deposited on a SiO_2/Si wafer using a UHV electron beam evaporation system (ULS 400, Balzers). The carbon species were then squeezed out of Ni film in the form of single- or few-layer graphene by annealing at 1100 °C and $<1 \times 10^{-4}$ Pa for 5 min, followed by fast cooling. Both CVD-graphene and segregated graphene were transferred to the desired

substrates using the nanotransfer-printing technique we developed.[30] All the graphene samples grown by CVD and segregation have a thickness of 1−3 layers over 82%. The RGO film was obtained by reducing graphene oxide (GO) film at 1000 °C in N_2 and H_2 (1:1) for 20−40 min, where GO was synthesized from natural graphite powder by a modified Hummers method.[31] The electrical conductivity of the obtained RGO film was ca. 10^5−10^6 ohm/square. For investigating the photocatalytic reaction anisotropy, thick, highly oriented pyrolytic graphite was utilized. In addition, ultralong carbon nanotubes used for fabricating all-carbon field effect transistors (FETs) were synthesized by catalytic CVD using CH_4 as the carbon source. A $FeCl_3$ aqueous solution (0.005 M) was applied to one edge of a SiO_2/Si substrate by microcontact printing, which serves as the catalyst precursor. The carbon nanotubes were grown at 980 °C with 15 sccm H_2 and 3 sccm CH_4 for 30 min. Well-separated carbon nanotube arrays can be grown on the SiO_2/Si substrate with nanotube lengths up to centimeters long.

Photocatalytic Experiments and Characterization. A xenon lamp (CHF-XM35−500 W) was employed as the light source of the photocatalytic reaction, in which wavelength >410 nm light was filtered. The photocatalytic reaction of graphene was performed in a homemade cylindrical quartz vessel (85 mm ×100 mm). The relative humidity was generally controlled by introducing an air-flow carrying water vapor while the O_2 content was regulated by using ordinary air, pure O_2, and pure N_2 gas. An optical microscope (Olympus DX51), scanning electron microscope (Hitachi S-4800), and atomic force microscope (Veeco Nanoscope III) in tapping mode were used for morphology studies of graphene. Raman spectroscopy (Renishaw RM1000) with laser excitation energy of 632.8 nm (1.96 eV) was used to evaluate the tailoring results. UV−vis spectra of CVD-graphene on quartz plates under different experimental conditions were recorded with a Perkin Elmer Lambda 950 UV/vis spectrometer. All the electrical measurements were carried out on a Keithley 4200 system.

■ RESULTS AND DISCUSSION

The TiO_2 photomask is the key to photocatalytic graphene engineering. An effective photomask has a sandwiched structure, including the quartz plate/5−15 nm TiO_2/75−90 nm patterned Cr. The TiO_2 film was prepared by vacuum-evaporating Ti on quartz, followed by calcination in air at 600 °C for 1 h. The patterned Cr film, fabricated by conventional lithographic techniques, serves as both the shielding mask of light and the quencher of the surrounding photogenerated electrons, holes, ·OH, and $O_2^{\bullet-}$ for the effective confinement of the photocatalytic reaction on graphene. Figure 1b−d demonstrates various types of photocatalytically patterned graphene produced by segregation (b), chemical vapor deposition (CVD) (c), and reduction of graphene oxide (d). The cutting was simply performed by putting the patterned TiO_2 photomask onto graphene with the Cr side facing the graphene, followed by Xe-lamp irradiation for 75 to 90 minutes under ambient conditions. As shown in the inset of Figure 1b, the intensity of the Raman G band along the arrow direction sharply dropped to zero at the photoexposed area, indicative of the complete decomposition of the graphene carbon network defined by the photomask patterns. This photocatalytic graphene cutting can be performed on arbitrary substrates, including a SiO_2/Si wafer (Figure 1b−d) or a plastic surface (Figure 1e), which offers great freedom for fabricating graphene-based flexible and transparent electronic devices. The cutting size feature is determined by the photomask as demonstrated in Figure 1f, where graphene ribbons of various widths have been obtained by using a line-shaped photomask having different line widths.

Different from conventional e-beam lithography and photolithography,[5] the photocatalytic cutting is a solution- and chemical-free process that does not introduce any photoresist or other chemical reagents. This is of particular importance for graphene electronics because any chemical contamination would degrade the device performance. Figure 2 compares the cutting performance of graphene at edge regions for TiO_2 photocatalysis (a), e-beam lithography (b), and photolithography (c), where the latter two approaches were followed by oxygen plasma etching as usual. Lots of contaminant spots, mostly originating from the photoresist residues, are observed over the e-beam- and photolithography-treated graphene surface (see Figure 2b,c). Such kinds of chemical contaminants cannot easily be removed even after vacuum-annealing for 1 h at 700 °C (see Figure 2e,f). In contrast, the convenient photocatalytic approach did not involve any photoresist, thus leading to a clean cutting of graphene. Because the photocatalytic cutting is an oxidative process, the cutting edge of graphene would be terminated by carbonyl, hydroxyl, and carboxyl groups, similar to oxygen plasma etching.[32] After vacuum-annealing treatment, the cutting edge was further sharpened to some extent as shown in Figure 2d. Different from the metal nanoparticle-guided crystallographic hydrogenative cutting,[14−16] the photocatalytic cutting would most possibly lead to a mixed zigzag and armchair edge structure. However, the advantage of photocatalytic cutting over the nanoparticle approach is its easy handling, excellent controllability, and compatibility to the current fabrication technology. It should be pointed out that the apparent rough edges obtained in some cases are originating from the inhomogeneous layer distribution of graphene samples because of the thickness effect on the photocatalytic etching rate. Using the RGB (red/green/blue) color distribution mode of optical microscope images, the effect of layer thickness on etching rate is clearly illustrated in Figure 2g. The thicker the film region, the smaller the etching rate, and thus more graphene materials remain.

The photocatalytic reaction of graphene is a progressive oxidation process accompanied by introduction of oxy groups such as epoxy, hydroxyl, carbonyl, and carboxyl groups and bond breaking of the sp^2 carbon network.[24] This provides an alternative way to tailor the graphene sheet by chemical patterning instead of actual cutting, simply by controlling the extent of photocatalytic reaction. Of particular importance is the localized conversion of conducting graphene to insulating graphene oxide by shortening the reaction time as schematically shown in Figure 3a. Using a circular pattern TiO_2 photomask, we have fabricated a regular GO dots array on monolayer graphene as shown in Figure 3b. At the photoexposed area, the Raman D band of graphene emerges and increases with irradiation time (see Supporting Information Figure S1) while the Raman spectrum of the Cr-covered unexposed region remains intact (see inset of Figure 3b). Hence, the GO dots can be easily visualized by mapping the Raman D to G band intensity ratio. As shown in the AFM image of Figure 3c, formation of GO dots did not break the physical intactness of graphene. Certainly, an intensive light irradiation will ultimately burn holes on the graphene sheet as described above. We monitored the sheet resistance change of graphene upon TiO_2-aided irradiation with a Hall bar device and four probe measurements. The typical result is given in Figure 3d. After the initial induction stage, the electrical resistance of graphene film exhibits a rapid increase in response to light irradiation. The resistance value was up to a level of 10^9 ohm/square, suggesting the formation of graphene oxide.[33,34] Raman
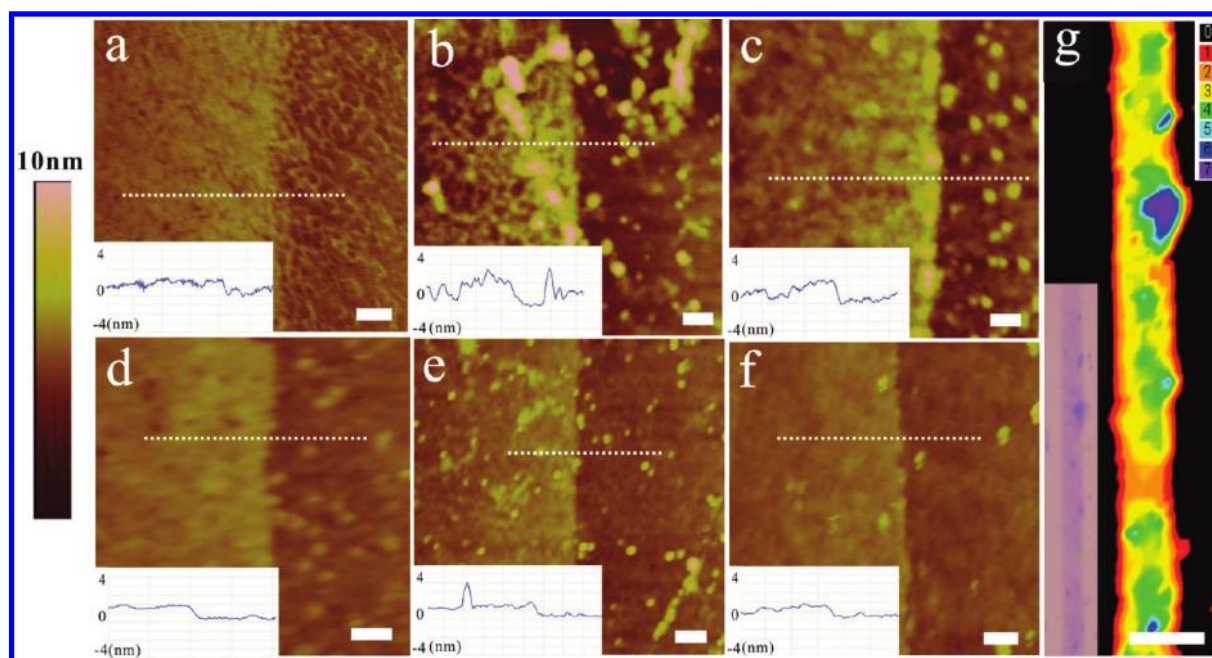
Figure 2. Edge structures of graphene ribbons obtained with different cutting techniques. Atomic force microscopy images of graphene ribbon edges with a−c being fabricated by photocatalytic cutting, e-beam lithography and photolithography, respectively, and d−f being the corresponding results after vacuum-annealing treatment at 700 °C for 1 h. Insets, the height profiles taken along the dotted lines. (g) RGB color distribution of the optical microscope image demonstrating the thickness effect on photocatalytic etching rate of graphene. The layer thickness is represented by different colors as shown in the upper inset color codes. The lower inset shows the unprocessed optical microscope image of g. Scale bars: 50 nm (a−f), 20 μm (g).
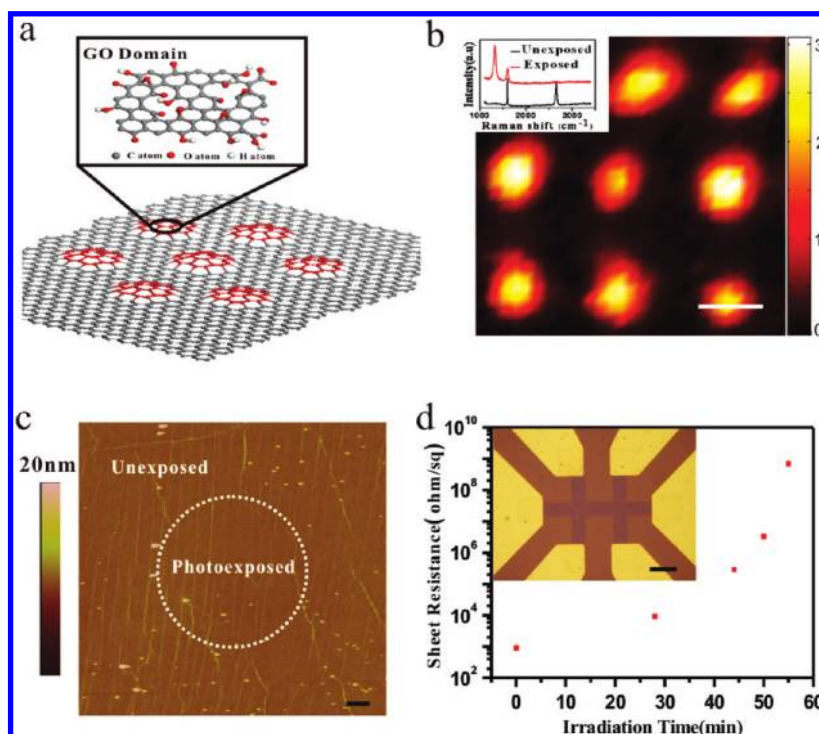
Figure 3. Localized graphene to graphene oxide conversion with a controlled photocatalysis. (a) Cartoon drawing of photocatalysis-induced GO patterns on graphene. (b) D/G intensity ratio mapping of CVD-graphene after mild photocatalytic treatment using a circular TiO$_2$ photomask, where the inset exhibits the Raman spectra of photoexposed and Cr-covered unexposed areas. (c) AFM image of GO-patterned graphene showing the intact film structure. (d) Change of graphene sheet resistance in response to light irradiation time with an unpatterned TiO$_2$ film/quartz plate photomask, where the inset shows the device structure for electrical measurement. Scale bars: 5 μm (b); 1 μm (c); 20 μm (inset of d).

mapping data indicate that the photoexposed graphene film remains intact at this stage (see Supporting Information Figure S2).

The controllable localized conversion of graphene to insulating graphene oxide on a graphene sheet provides great versatility for
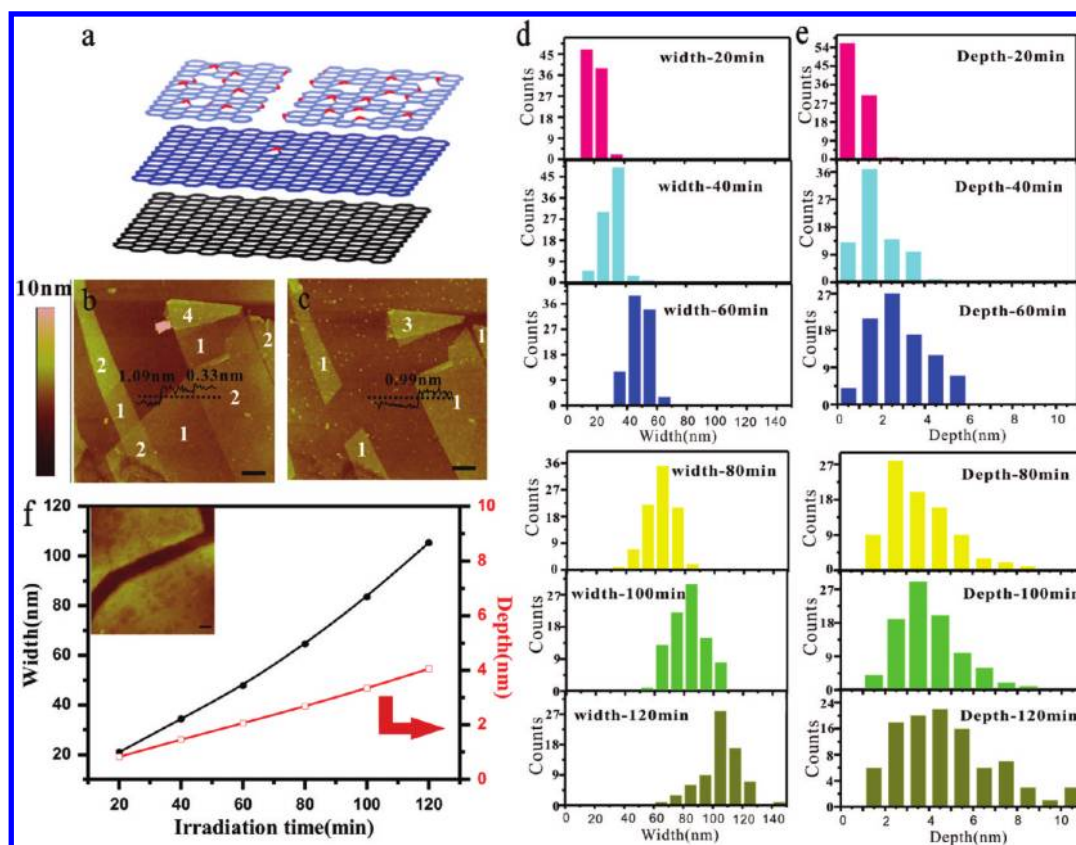
Figure 4. Photocatalytic layer-by-layer thinning of few-layer graphene. (a) Schematic of layer-by-layer thinning reaction. (b and c) AFM images of mechanically exfoliated graphene before and after photocatalytic treatment, respectively, in which the labeled numbers correspond to the layer thickness and the insets show the height profiles taken along the dotted lines. (d and e) Histograms of crack width (d) and depth (e) on thick graphite at different irradiation times (see inset of f). (f) Dependence of crack width and depth on thick graphite on UV irradiation time. Scale bars: 1 μm (b, c), 50 nm (inset of f).

creating graphene-based electronic devices. For the zero-gap graphene, it is vital to open the bandgap either by cutting into the nanoribbons or by creating a periodic holes array.[5,7−11] The "virtual" cutting by forming highly insulating graphene oxide on graphene sheets would avoid the troublesome edge problems, including edge passivation,[35,36] uncertain edge geometry,[37] etc. The introduction of various reactive oxy groups by TiO_2 photocatalysis also offers a useful platform for further chemical functionalization of graphene. It therefore provides considerable opportunity for the development of graphene-based electronic and luminescent devices.[38,39]

The chemical reactivity of graphenic carbon bonds is extremely low.[40] In fact, the existence of the induction stage corresponding to a slow resistance change upon light illumination is an indication of the chemical inertness of graphene. The photocatalytic reaction of a perfect graphenic carbon network requires large activation energy. Once defects and pinholes are generated on the graphene surface, the oxidative reaction would proceed very rapidly along these reactive sites, leading to the sharp increase of electrical resistance. This suggests a possibility of photocatalytic layer-by-layer thinning of few-layer graphene as illustrated in Figure 4a in view of the fact that the reaction always starts from the top layer. Shown in Figure 4c is the successful example obtained from mechanically exfoliated few-layer graphene. Comparing the AFM images in Figure 4b and 4c, we clearly see that one monolayer has been peeled off from each few-layer graphene after TiO_2-aided irradiation. The coexistence of

various graphene flakes with different layer thicknesses facilitated the identification of such photocatalytic layer-by-layer exfoliation. Accompanied with the disappearance of monolayer graphene (ca. 1 nm thick in AFM height image on SiO_2/Si substrate), the layer thicknesses of other multilayer flakes decrease by a value of 0.32−0.45 nm, which is well consistent with one-layer thinning.[41] The exposed fresh surfaces have similar AFM topography with pristine graphene though some defects were induced as demonstrated by the emergence of Raman D band. To quantitatively evaluate the rate difference of in-plane and out-of-plane photocatalytic etching, we followed the etching process on thick graphite by AFM imaging and paid particular attention to a surface crack as shown in the inset of Figure 4f. Compared with the surface-grown graphene, the highly oriented pyrolytic graphite is more suitable for the reaction anisotropy study because of the lack of defects. Upon light irradiation, this surface crack becomes wider and deeper, indicating that both in-plane and out-of-plane etching reactions have been proceeding. Figure 4d−f reveals the histograms of crack width and depth changes and their correlations with irradiation time. As expected, the out-of-plane reaction is much slower than the in-plane reaction, with the former being roughly a linear process while the latter is an accelerating process. Obviously the ratio of the slopes of the two plots is a simple measure of the etching rate difference, which is 9.4 at the initial reaction stage and reaches 18.7 after 2h irradiation. Therefore, we conclude that the in-plane photocatalytic etching rate is at least 1 order of magnitude higher than
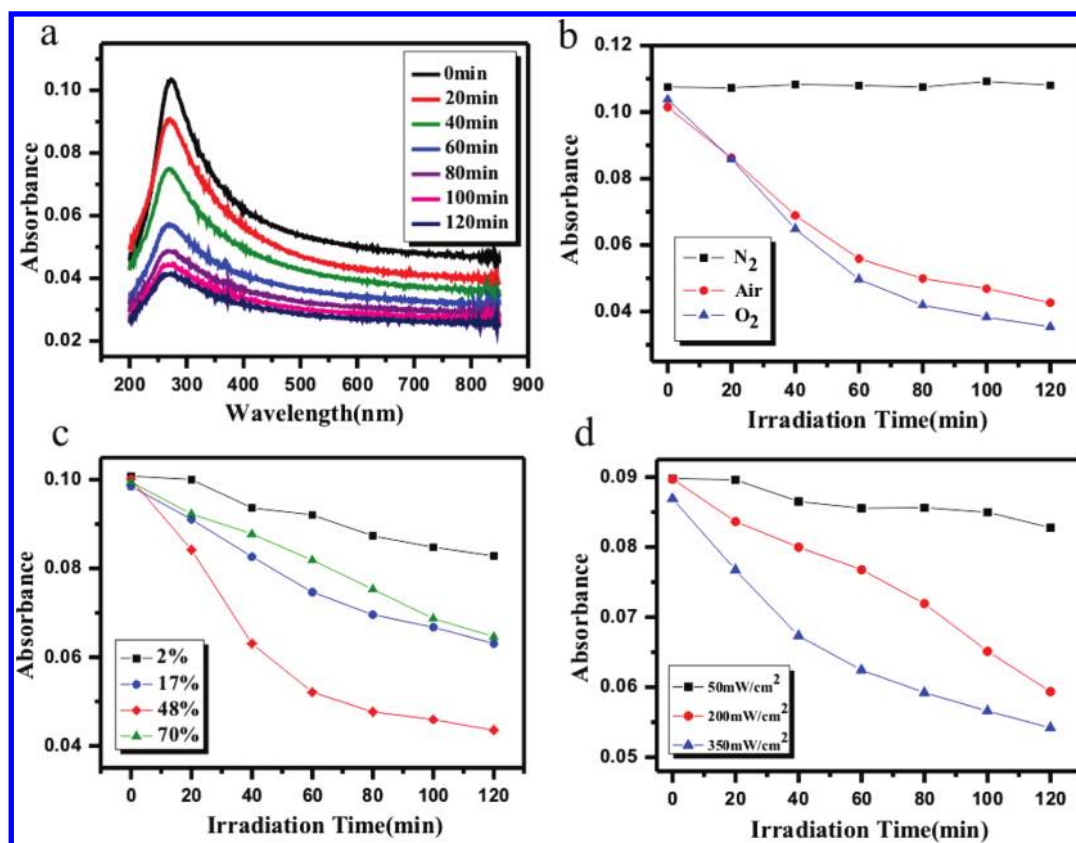
Figure 5. Effect of O_2 and humidity on photocatalytic graphene tailoring. (a) UV−vis absorption spectra of CVD-graphene grown on Ni corresponding to TiO_2-aided light irradiation. Change of absorbance at λ_{max} around 273 nm in response to irradiation time under different O_2 partial pressures (b), relative humidities (c), and light intensities (d). The experimental conditions were 50% RH, 350 mW/cm^2 (b), 350 mW/cm^2 in air (c), and 50% RH in air (d).

the out-of-plane etching at the experimental time scale. This remarkable difference of etching rate enables the layer-by-layer thinning of few-layer graphene.

The photocatalytic reaction of graphene involves oxygen and water vapor in the surroundings. We employed UV−vis spectroscopy to monitor the reaction process under different experimental conditions to understand the effects of oxygen partial pressure and relative humidity (RH). The UV−vis absorption spectrum of graphene is characteristic of a broad transition band centered at ca. 273 nm as shown in Figure 5a, which is attributed to the π−π^* transition of electrons in graphene associated with plasmon resonance.[42,43] This absorption band exhibits a gradual decrease in intensity and a blue-shift upon light illumination, suggesting that the electronic conjugation within the graphene sheet has been gradually destroyed by photocatalytic etching.[43] In the control experiment, no discernible spectral change was observed under 2 h UV irradiation without using TiO_2 photocatalyst film (see Supporting Information Figure S3), which confirms that TiO_2 photocatalysis is essential for the graphene tailoring rather than a general UV degradation effect. To examine the effect of oxygen, we carried out the photocatalytic reaction of graphene in N_2, O_2, and air, all at 50% RH. As seen from the absorption peak intensity versus irradiation time plot in Figure 5b, no discernible reaction occurred under N_2 atmosphere, indicating that O_2 molecules are indispensable for the photocatalytic reaction. On the other hand, irradiation under O_2 and air both led to a rapid decrease in absorption peak intensity. Previous study of Berger et al.[44] suggested that the effect of

oxygen on TiO_2 photocatalysis has a saturation point of partial pressure, which is approximately 25 mbar, much below that in air. This can well explain the slight difference of absorbance change under O_2 and air observed in our work. It also indicates that the ambient condition can supply enough oxygen molecules to pursue an effective photocatalytic tailoring of graphene. The humidity effect was investigated similarly as shown in Figure 5c. The reaction rate, indicated by the slope of absorbance vs irradiation time curve, increases monotonically together with the increase of relative humidity in air. However, this trend stops at ca. 50%. At a higher relative humidity, the reaction kinetics was remarkably slowed down. For instance, the reaction rate at 70% RH was even smaller than that at 17% RH. Moreover, the influence of UV light intensity was also examined, and the result was summarized in Figure 5d. Similar to other photocatalytic reactions,[45] the increase of light intensity led to a faster reaction rate. The photocatalytic reaction can proceed remarkably at a light intensity as low as 50 mW/cm^2 in air and 50% RH. In brief, the TiO_2-based photocatalytic tailoring of graphene is feasible under a wide range of humidity, oxygen partial pressure, and light intensity, with the recommended experimental conditions being ca. 50% RH in air.

TiO_2 has two typical crystal forms, anatase and rutile with a bandgap of 3.2 and 3.0 eV, respectively. As confirmed by TEM and Raman data (see Supporting Information Figure S4), both anatase and rutile forms coexisted in our vacuum-evaporated TiO_2 thin film. Previous studies prove that the photogenerated e^- and h^+ are trapped at Ti (IV) and bridging oxygen sites,
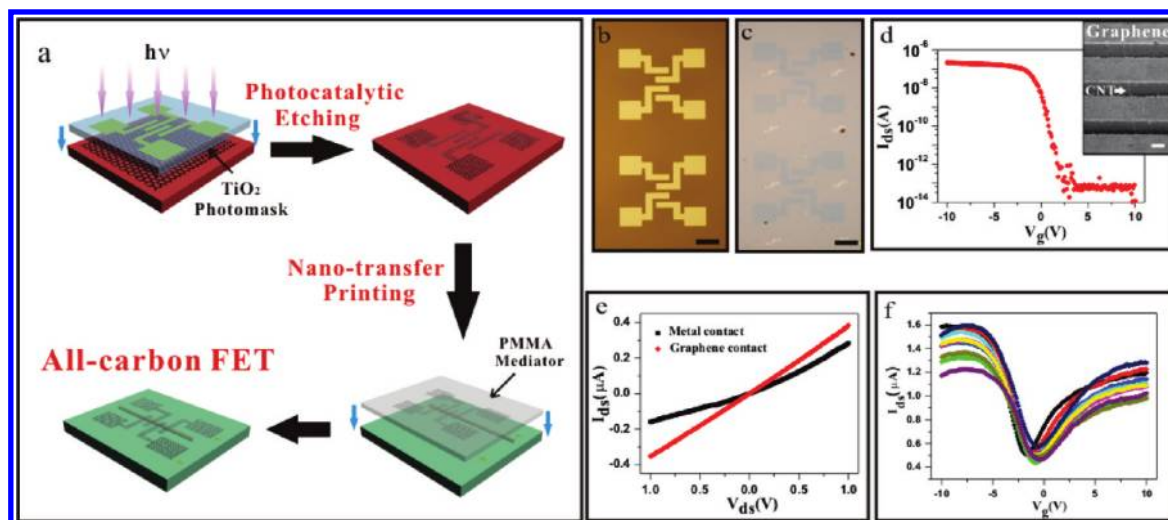
Figure 6. All-carbon FET array fabricated by the photocatalytic patterning approach. (a) Schematic of device fabrication procedure. Optical microscope images of TiO_2 photomask (b) and the obtained graphene electrode patterns (c). (d) $I_{ds}-V_g$ curve (at $V_{ds} = 0.1$ V) of an all-carbon FET with a semiconducting carbon nanotube serving as the conduction channel. Inset, SEM image of the device. (e) $I_{ds}-V_{ds}$ curves (at $V_g = -10$ V) of a semiconducting FET with graphene (red) and metal (black, 8 nm-Cr/50 nm-Au) contacts. (f) $I_{ds}-V_g$ curves (at $V_{ds} = 0.1$ V) of the all-carbon FETs with an ultralong metallic carbon nanotube across many groups of graphene electrodes. Scale bars: 100 μm (b, c), 20 μm (inset of d).

respectively, which lead to the weakening of Ti—O bonds. As a result, oxygen atoms are released and oxygen vacancies are created.[46] Water molecules can be preferentially adsorbed onto these oxygen vacancies, producing adsorbed OH groups.[47] The high energy holes (having a redox potential of +2.53 V vs NHE) oxidize the adsorbed OH groups and H_2O molecules, creating highly reactive hydroxyl radicals ($\cdot$OH). On the other hand, the trapped electrons reduce the surrounding oxygen molecules into superoxide radicals ($O_2^{\bullet-}$), which further react with H_2O molecules, forming H_2O_2. The neutral H_2O_2 species further photodecompose into $\cdot$OH radicals under UV illumination.[46,48] Oxygen molecules play a key role in the photocatalytic tailoring reaction of graphene, which efficiently prevent photogenerated e^- and h^+ from recombination via electron capturing and also create the most important $\cdot$OH radicals. It is believed that these highly reactive $\cdot$OH radicals work as the actual photoscissors of graphenic carbon network.[48] The etching rate decrease at high relative humidity would be attributed to the shielding effect of a thick water layer on the access of oxygen molecules to surface-trapped electrons.

It should be pointed out that although there are two different routes to generate $\cdot$OH radicals, the H_2O_2 photodecomposition route would mainly contribute to the graphene tailoring, determined by our TiO_2 photomask structure. With a TiO_2 photomask directly patterned on a quartz plate, the photodegraded area of the graphene sheet was found to far exceed the feature size of the mask pattern. For instance, no graphene ribbons remained when the photomask spacing between TiO_2 stripes was less than 10 μm, which is obviously attributed to the surface diffusion of H_2O_2 species and subsequent photodecomposition to $\cdot$OH radicals. In contrast, a sandwiched photomask structure of quartz plate/TiO_2 film/patterned Cr film led to a well-controlled patterning of the graphene sheet. In this case, the Cr layer is believed to serve as a light shield and a radical quencher to avoid unexpected overetching of graphene. As a consequence, a suitable design of TiO_2 photomask is essential for performing the photocatalytic graphene engineering.

The photocatalytic tailoring technique provides versatile possibilities for fabricating graphene devices. We constructed here a FET array as a demonstration. As schematically shown in Figure 6a, the graphene sheet on the SiO_2/Si wafer was first photocatalytically patterned into the electrode structure using the TiO_2 photomask (see Figure 6b and 6c). The graphene electrodes were then transferred onto an individual carbon nanotube using the nanotransfer-printing technique we developed recently.[49] By simply using such a two-step procedure, we can achieve an all-carbon FET array, in which the patterned graphene serves as the source (S) and drain (D) electrodes, the carbon nanotube as the conduction channel, a p^{+2} silicon as the back gate, and a thermally grown 300 nm SiO_2 as the gate dielectrics (see inset of Figure 6d; channel length $L = 20$ μm). Considering the mild photocatalytic etching process, it is no doubt that similar work can be performed on plastics for fabricating flexible and transparent devices.[50] Figure 6d shows the typical transfer characteristics of the fabricated all-carbon FETs with a semiconducting tube, which exhibits a unipolar p-channel behavior with an on/off current ratio of >10^5. Different from the conventional Au/Cr electrode, the graphene—carbon nanotube interface shows a symmetric ohmic contact as demonstrated by the linear $I_{ds}-V_{ds}$ curve (Figure 6e). On the other hand, all-carbon FETs with a metallic tube exhibit an ambipolar performance as shown in Figure 6f. Measurements of an ultralong metallic tube across different groups of graphene electrodes demonstrated good reproducibility of the graphene—carbon nanotube contacts. The obtained high performances of these all-carbon FETs benefit from the clean and dry feature of our photocatalytic etching technique which is free from possible chemical contaminations.

■ CONCLUSIONS

In brief, we have demonstrated a facile way to engineer the single- and few-layer graphene using TiO_2 photocatalysis. This clean and dry photocatalytic process enables a versatile tailoring of graphene, including ribbon cutting, arbitrary patterning,

layer-by-layer thinning, localized graphene to graphene oxide conversion, etc. Different from the existing techniques, the TiO_2-based photocatalytic patterning and modification approach is easy, cost-effective, free from chemical contamination, and universal to various substrates, offering great opportunity for fabricating graphene devices. We believe that it would greatly contribute to the graphene electronics, a most promising area of graphene research.

■ ASSOCIATED CONTENT

ⓢ Supporting Information. Complete ref 32. Time evolution of the Raman spectrum for a single layer graphene during photocatalytic reaction. Raman mapping of photoconverted graphene oxide in the Hall bar device. UV irradiation effect on graphene without using TiO_2 photomask. AFM and TEM characterization as well as Raman and UV spectra of the TiO_2 film. This material is available free of charge via the Internet at http://pubs.acs.org.

■ AUTHOR INFORMATION

Corresponding Author
zfliu@pku.edu.cn

Present Addresses
§Present address: Department of Chemistry and Chemical Biology, Harvard University, Cambridge, MA 02138.

■ ACKNOWLEDGMENT

■ REFERENCES

(1) Geim, A. K.; Novoselov, K. S. Nat. Mater. 2007, 6, 183–191.
(2) Zhang, Y.; Tan, Y.; Stormer, H. L.; Kim, P. Nature 2005, 438, 201–204.
(3) Bolotin, K. I.; Sikes, K. J.; Jiang, Z.; Klima, M.; Fudenberg, G.; Hone, J.; Kim, P.; Stormer, H. L. Solid State Commun. 2008, 146, 351–355.
(4) Nair, R. R.; Blake, P.; Grigorenko, A. N.; Novoselov, K. S.; Booth, T. J.; Stauber, T.; Peres, N. M. R.; Geim, A. K. Science 2008, 320, 1308.
(5) Han, M. Y.; Ozyilmaz, B.; Zhang, Y.; Kim, P. Phys. Rev. Lett. 2007, 98, 206805.
(6) Areshkin, D. T.; White, C. T. Nano Lett. 2007, 7, 3253–3259.
(7) Li, X.; Wang, X.; Zhang, L.; Lee, S.; Dai, H. Science 2008, 319, 1229–1232.
(8) Son, Y. W.; Cohen, M. L.; Louie, S. G. Phys. Rev. Lett. 2006, 97, 216803.
(9) Park, C. H.; Yang, L.; Son, Y. W.; Cohen, M. L.; Louie, S. G. Nat. Phys. 2008, 4, 213–217.
(10) Bai, J.; Zhong, X.; Jiang, S.; Duan, X. Nat. Nanotechnol. 2010, 5, 190–194.
(11) Kim, M.; Safron, N. S.; Han, E.; Arnold, M. S.; Copalan, P. Nano Lett. 2010, 10, 1125–1131.
(12) Tapaszto, L.; Dobrik, G.; Lambin, P.; Biro, L. P. Nat. Nanotechnol. 2008, 3, 397–401.
(13) Weng, L.; Zhang, L.; Chen, Y. P.; Rokhinson, L. P. Appl. Phys. Lett. 2008, 93, 093107.
(14) Datta, S. S.; Strachan, D. R.; Khamis, S. M.; Johnson, A. T. C. Nano Lett. 2008, 8, 1912–1915.
(15) Ci, L.; Xu, Z.; Wang, L.; Gao, W.; Ding, F.; Kelly, K. F.; Yakobson, B. I.; Ajayan, P. M. Nano Res. 2008, 1, 116–122.
(16) Campos, L. C.; Manfrinato, V. R.; Sanchez-Yamagishi, J. D.; Kong, J.; Jarillo-Herrero, P. Nano Lett. 2009, 9, 2600–2604.
(17) Severin, N.; Kirstein, S.; Sokolov, I. M.; Rabe, J. P. Nano Lett. 2009, 9, 457–461.
(18) Cong, C.; Yu, T.; Ni, Z.; Liu, L.; Shen, Z.; Huang, W. J. Phys. Chem. C 2009, 113, 6529–6532.
(19) Bai, J.; Duan, X.; Huang, Y. Nano Lett. 2009, 9, 2083–2087.
(20) Fujishima, A.; Honda, K. Nature 1972, 238, 37–38.
(21) Fujishima, A.; Zhang, X.; Tryk, D. A. Surf. Sci. Rep. 2008, 63, 515–582.
(22) Fujishima, A.; Rao, T. N.; Tryk, D. A. J. Photochem. Photobiol. C 2000, 1, 1–21.
(23) Tatsuma, T.; Tachibana, S.; Miwa, T.; Tryk, D.; Fujishima, A. J. Phys. Chem. B 1999, 103, 8033–8035.
(24) Tatsuma, T.; Tachibana, S.; Fujishima, A. J. Phys. Chem. B 2001, 105, 6987–6992.
(25) Hurum, D. C.; Agrios, A. G.; Gray, K. A. J. Phys. Chem. B 2003, 107, 4545–4549.
(26) Kubo, W.; Tatsuma, T. Anal. Sci. 2004, 20, 591–593.
(27) Reina, A.; Jia, X.; Ho, J.; Nezich, D.; Son, H.; Bulovic, V.; Dresselhaus, M. S.; Kong, J. Nano Lett. 2009, 9, 30–35.
(28) Li, X.; Cai, W.; An, J.; Kim, S.; Nah, J.; Yang, D.; Piner, R.; Velamakanni, A.; Jung, I.; Tutuc, E.; Banerjee, S. K.; Colombo, L.; Ruoff, R. S. Science 2009, 324, 1312–1314.
(29) Liu, N.; Fu, L.; Dai, B.; Yan, K.; Liu, X.; Zhao, R.; Zhang, Y.; Liu, Z. Nano Lett. 2011, 11, 297–303.
(30) Jiao, L.; Fan, B.; Xian, X.; Wu, Z.; Zhang, J.; Liu, Z. J. Am. Chem. Soc. 2008, 130, 12612–12613.
(31) Hummers, W. S.; Offeman, R. E. J. Am. Chem. Soc. 1958, 80, 1339.
(32) Guo, X.; et al. Science 2006, 311, 356–359.
(33) Gomez-Navarro, C.; Weitz, R. T.; Bittner, A. M.; Scolari, M.; News, A.; Burghard, M.; Kern, K. Nano Lett. 2007, 7, 3499–3503.
(34) Wu, X.; Sprinkle, M.; Li, X.; Ming, F.; Berger, C.; de Heer, W. A. Phys. Rev. Lett. 2008, 101, 026801.
(35) Barone, V.; Hod, O.; Scuseria, G. E. Nano Lett. 2006, 6, 2748–2754.
(36) Li, Z.; Yang, J.; Hou, J. J. Am. Chem. Soc. 2008, 130, 4224–4225.
(37) Koskinen, P.; Malola, S.; Hakkinen, H. Phys. Rev. B 2009, 80, 073401.
(38) Gokus, T.; Nair, R. R.; Bonetti, A.; Bohmler, M.; Lombardo, A.; Novoselov, K. S.; Geim, A. K.; Ferrari, A. C.; Hartschuh, A. ACS Nano 2009, 3, 3963–3968.
(39) Eda, G.; Lin, Y. Y.; Mattevi, C.; Yamaguchi, H.; Chen, H. A.; Chen, I. S.; Chen, C. W.; Chhowalla, M. Adv. Mater. 2010, 22, 505–509.
(40) Wang, X.; Dai, H. Nature Chem. 2010, 2, 661–665.
(41) Geringer, V.; Liebmann, M.; Echtermeyer, T.; Runte, S.; Schmidt, M.; Ruckamp, R.; Lemme, M. C.; Morgenstern, M. Phys. Rev. Lett. 2009, 102, 076102.
(42) Yang, L.; Deslippe, J.; Park, C. H.; Cohen, M. L.; Louie, S. G. Phys. Rev. Lett. 2009, 103, 186802.
(43) Li, D.; Muller, M. B.; Gilje, S.; Kaner, R. B.; Wallace, G. G. Nat. Nanotechnol. 2007, 3, 101–105.
(44) Berger, T.; Sterrer, M.; Diwald, O.; Knozinger, E. Chem. Phys. Chem. 2005, 6, 2104–2112.
(45) Tastuma, T.; Kubo, W.; Fujishima, A. Langmuir 2002, 18, 9632–9634.
(46) Carp, O.; Huisman, C. L.; Reller, A. Prog. Solid State Chem. 2004, 32, 33–177.
(47) Bikondoa, O.; Pang, C. L.; Ithnin, R.; Muryn, C. A.; Onishi, H.; Thornton, G. Nat. Mater. 2006, 5, 189–192.
(48) Kubo, W.; Tatsuma, T. J. Am. Chem. Soc. 2006, 128, 16034–16035.
(49) Jiao, L.; Xian, X.; Wu, Z.; Zhang, J.; Liu, Z. Nano Lett. 2009, 9, 205–209.
(50) Cao, Q.; Hur, S. H.; Zhu, Z. T.; Sun, Y.; Wang, C.; Meitl, M. A.; Shim, M.; Rogers, J. A. Adv. Mater. 2006, 18, 304–309.